Influence of Y2O3 addition on the mechanical and oxidation behaviour of carbon fibre reinforced ZrB2/SiC composites

Original
Influence of Y2O3 addition on the mechanical and oxidation behaviour of carbon fibre reinforced ZrB2/SiC composites / Vinci, A.; Zoli, L.; Galizia, P.; Sciti, D.. - In: JOURNAL OF THE EUROPEAN CERAMIC SOCIETY. - ISSN 0955-2219. - STAMPA. - 40:15(2020), pp. 5067-5075. [10.1016/j.jeurceramsoc.2020.06.043]

Availability:
This version is available at: 11583/2952111 since: 2022-01-21T14:35:49Z

Publisher:
Elsevier Ltd

Published
DOI:10.1016/j.jeurceramsoc.2020.06.043

Summary of novel conclusions

- Y_2O_3 forms liquid phases with impurity oxides and improves sintering
- Y-based liquid phases are further reduced by carbon to produce high melting phases
- The addition of Y_2O_3 leads to full density and a significant increase of the mechanical properties
- The collateral consumption of SiC leads to inferior oxidation resistance at 1650°C

Influence of Y_2O_3 addition on the mechanical and oxidation behaviour of carbon fibre reinforced ZrB_2/SiC composites

Antonio Vinci

CNR-ISTEC, Institute of Science and Technology for Ceramics, Via Granarolo 64, I-48018 Faenza, Italy

antonio.vinci@istec.cnr.it

Luca Zoli

CNR-ISTEC, Institute of Science and Technology for Ceramics, Via Granarolo 64, I-48018 Faenza, Italy

luca.zoli@istec.cnr.it

Pietro Galizia

CNR-ISTEC, Institute of Science and Technology for Ceramics, Via Granarolo 64, I-48018 Faenza, Italy

pietro.galizia@istec.cnr.it

Diletta Sciti

CNR-ISTEC, Institute of Science and Technology for Ceramics, Via Granarolo 64, I-48018 Faenza, Italy

diletta.sciti@istec.cnr.it

Abstract

The influence of Y2O3 addition on the microstructure, thermo-mechanical properties and oxidation resistance of carbon fibre reinforced ZrB2/SiC composites was investigated. Y2O3 reacted with oxide impurities present on the surface of ZrB2 and SiC grains and formed a liquid phase, effectively lowering the sintering temperature and allowing to reach full density at 1900°C. The presence of a carbon source (fibres) led to additional reactions which resulted in the formation of new secondary phases such as yttrium boro-carbides. Mechanical properties were significantly enhanced compared to the un-doped composite. Further tests at high

temperatures resulted in strength increase up to 700 MPa at 1500°C which was attributed to stress relaxation. Oxidation tests carried out at 1500°C and 1650°C in air showed that the presence of the Y-based secondary phases enhanced the growth of ZrO2 grains, but offered limited protection to oxygen due to the lower availability of surficial SiO2 formed from SiC.

Keywords

Ceramic-Matrix Composites (CMCs); Ultra-High-Temperature-Ceramics (UHTCs); Fibre-matrix interface; Rare Earths; Oxidation Resistance;

1. Introduction

The demand for materials able to withstand more challenging and harsh conditions than those encountered during re-entry in earth atmosphere or hypersonic flight, and surpass the current limits of C/SiC based CMCs, has driven researchers towards the study of a novel class of refractory ceramics called ultra-high temperature ceramics (UHTCs). These comprise the carbides and borides of early transition metals which are characterized by melting points above 3000°C and are being considered as candidates for the application in extreme environments. Amongst UHTCs, ZrB_2 is the most commonly studied due to its relatively low density, high thermal conductivity, and lower price compared to HfB_2 [1,2]. The main drawback is the low fracture toughness of these materials that limits their application where thermal shocks and vibrations are present [3]. Moreover the oxidation resistance of pure ZrB_2 is poor because of the formation of a porous and non-protective ZrO_2 scale and the evaporation of B_2O_3 already at 1000°C. In this regard, many efforts were made to overcome the low oxidation resistance of ZrB_2 by introducing additives, such as SiC and other silicides, which promote the formation of a surficial glassy silica phase which protects the material from further oxidation up to ∼1600°C. In order to improve the damage tolerance of these materials, short and long carbon fibres have been extensively investigated as reinforcement [4][5][6][7][8][9][10][11][12][13][14]. Results show how the introduction of the fibre reinforcement lowers the overall strength of the composite but greatly improves the damage tolerance and thermal shock resistance. Recently these materials were validated in an arc-jet wind tunnel facility and are currently being scaled up [15][16]. The main issues encountered during the fabrication of fibre reinforced UHTCs are typically related to the problematic infiltration of the fibre preforms and the consolidation of the green composite. Studies on the sintering behaviour of these composites showed how temperatures above 1900°C allowed to reach higher densities but severely damaged fibres in the process, therefore the addition of sintering aids was further investigated.

Rare earth oxides such as Y_2O_3 have been shown to improve the densification of ZrB_2/SiC bulk composites and allow to reach near full density ceramics due to the formation of a liquid phase with the oxide impurities present on the surface of ZrB_2 and SiC grains [17][18]. Moreover the presence of Y_2O_3 is thought to stabilize the ZrO_2 formed during oxidation in the tetragonal structure, leading to the formation of a more compact scale [19]. However, the effect of Rare Earth oxides on complex systems such as fibre reinforced UHTCs, where carbon is also present, has been never investigated.

In this work, 5 vol% Y_2O_3 was added to Cf reinforced ZrB_2-SiC composites in order to improve densification and oxidation resistance. The effect of Y_2O_3 on the microstructure, high temperature mechanical behaviour and oxidation resistance up to 1650°C was investigated.

2. Experimental

2.1. Raw materials

For the preparation of the ceramic suspensions, raw powders available commercially were used. The raw materials used were: ZrB_2 (H.C. Starck, grade B, Germany, specific surface area 1.0 m^2/g, particle size range 0.5-6 µm, impurities (wt.%): 0.25 C, 2 O, 0.25 N, 0.1 Fe, 0.2 Hf), α-SiC (H.C. Starck, Grade UF-25, specific surface area 23-26 m^2/g, D50 0.45 µm, Italian retailer: Metalchimica), Y_2O_3 (H.C. Starck, 99.5%, Grade C, specific surface area 10-16 m^2/g, D50 0.90 µm, impurities (wt.%): 0.005 Al, 0.003 Ca, 0.005 Fe). Unidirectional high modulus carbon fibres (Granoch, Yarn XN80-6K fibres; E = 780 GPa, $\sigma_{tensile}$ = 3.4 GPa, Ø = 10 µm) were used as fibre reinforcement.

2.2 Processing

Two powder mixtures containing ZrB_2 + 5 vol% SiC (designated ZS) and ZrB_2 + 5 vol% SiC + 5 vol% Y_2O_3 (designated ZSY) were prepared by wet ball milling of the commercial powders for 24 h and then dried with a rotary evaporator. The composites were fabricated via slurry infiltration of the fibre bundles; the fibre layers were piled up in a 0/0° configuration and then cut into a 30 x 30 mm pellet [20]. The sample was hot pressed at 1900°C for both composites, using a pressure of 40 MPa and a holding time of 15 min, in accordance to previous studies [20].

2.3. Microstructure analysis

The microstructures of the sintered materials were analysed on polished and fractured surfaces with a field emission scanning electron microscope (FE-SEM, Carl Zeiss Sigma NTS Gmbh Öberkochen, Germany) and energy dispersive X-ray spectroscopy (EDX, INCA Energy 300, Oxford instruments, UK). X-ray diffraction analysis (Bruker D8 Advance apparatus, Karlsruhe, Germany) was carried out on the materials before and after oxidation tests. The bulk densities were determined from mass and geometric volumes. The fibre and matrix volumetric amounts were evaluated by image analysis with software Image-Pro Analyser 7.0 and the theoretical densities were calculated using the rule of mixtures. Relative density was calculated as the ration of bulk and theoretical density.

2.4. Mechanical testing

Flexural strength was measured by four-point bending on specimens with size $25 \times 2.5 \times 2$ mm^3 (Length × Width × Height) using a fully-articulated steel fixture and a screw-driven testing machine (Zwick/Roell, model Z050). The lower and upper span were 20 mm and 10 mm respectively, while the cross-head rate was 1 mm/min. The tests were carried out following the guidelines of standard EN 843-1 (2006). For the tests at 1200°C and 1500°C, a screw-driven testing machine (1195, INSTRON) was used; the specimens were placed on a semi-articulated alumina 4-point fixture and heated up to 1500°C with a rate of 10°C/min under argon flow (3.5 L/min) in a high temperature furnace (HTTF model 924, Severn Furnaces Limited). Bars were held at 1500°C for 15 min before testing.

The fracture toughness (K_{Ic}) was evaluated by 4-point bending on chevron notched beams (CNB), following the guidelines of EN 14425-3 (2010). The equation of Munz et al. was used to calculate K_{Ic} [21]. The test bars, $25 \times 2 \times 2.5$ mm^3 (Length × Width × Height), were notched with a 0.1 mm-thick diamond saw; the chevron-notch tip depth and average side length were about 0.12 and 0.80 of the bar thickness, respectively. The testing apparatus is the same used for RT flexural strength. A crosshead speed of 0.05 mm/min was used.

2.5. Short-term oxidation tests

Bars with dimensions 2.5 × 2 × 12 mm were machined from the sintered specimens. The samples were cleaned with ethanol and dried under IR light. The oxidation tests were carried out in a bottom-up loading furnace (FC18-0311281, Nannetti Antonio Sauro S.R.L., Italy) at 1500 and 1650°C in air for 1 min following the same procedure reported in [14]. The furnace was heated to the desired temperature with a rate of 5 °C/min. Then the specimens were placed in the furnace using a porous zirconia sample holder. After reaching the target temperature, the samples were held in the furnace for 1 min. At the end of the oxidation test, the specimens were quickly taken out and cooled down naturally in air.

3. Results and discussion

3.1 Microstructure of the sintered material

The physical properties of samples ZS and ZSY are reported in Table 1. The final densities ranged from 3.7 to 4 g/cm^3, depending on the amount of residual porosity and fibre volumetric content. The composites contained comparable amounts of fibres; slight deviations are due to the intrinsic variability and scatter of the manual process of infiltration.

Table 1. Values of density (theoretical, experimental and relative), porosity, fibre content, ZrB_2 grain size and the main phases identified by XRD and EDS analysis for samples ZS and ZSY

Sample	Composition (vol%)	$\rho_{theor.}$ (g/cm^3)	$\rho_{exp.}$ (g/cm^3)	$\rho_{rel.}$ (g/cm^3)	Porosity (vol%)	Fibre (vol%)	ZrB_2 grain size (µm)	XRD/EDS phases
ZS	ZrB_2 + 5 SiC	4.09	3.74	91.4	8.2	43.4	2.4	ZrB_2, SiC, ZrC
ZSY	ZrB_2 + 5 SiC + 5 Y_2O_3	4.01	3.99	99.9	0.1	48.9	3.6	ZrB_2, SiC, ZrC, Y-B-C-O

Sample ZS:

Fibres were homogeneously distributed in the ceramic matrix (fig. 1a), while SiC particles did not show any sign of coarsening, retaining their original size (fig. 1b). From the fibre regions, no evidence was found to indicate a strong chemical reaction between fibre and matrix as the fibres retained their original round shape (fig. 1c). Some ZrC particles, along with SiC, were observed at the fibre/matrix interface which originated from the reduction of impurity oxides (ZrO_2 and SiO_2) located in the proximity of the carbon fibres[22].

$$SiO_2 + 3\,C \rightarrow SiC + 2\,CO_{(g)}$$

$$ZrO_2 + C \rightarrow ZrC + CO_{(g)}$$

SiC volumetric content was quantified by image analysis after sintering and the measured content was ~5%, in accordance with the initial nominal amount (5%).

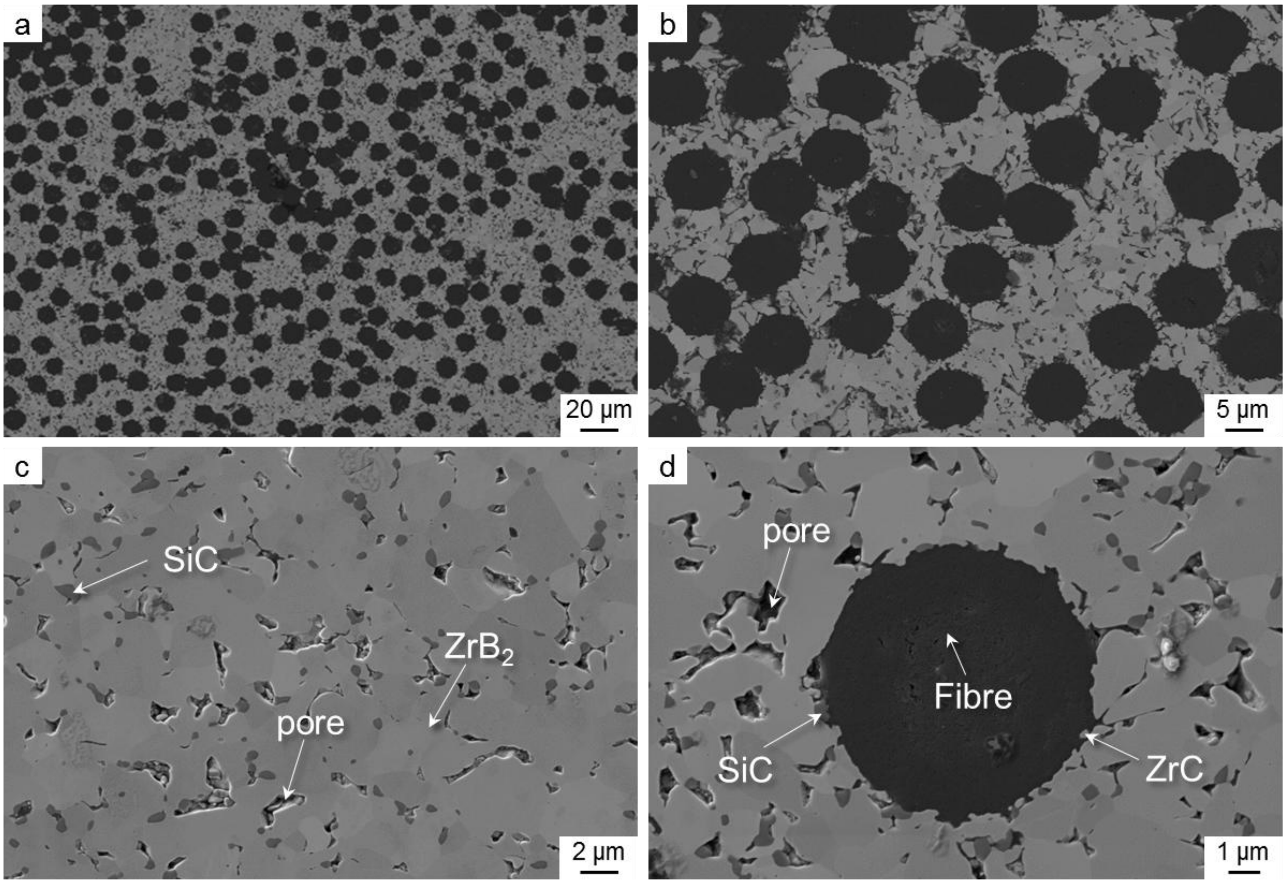

Figure 1. SEM micrographs of ZS: a) Fibre distribution, b) microstructure and phases distribution, c) detail of the UHTC matrix, d) Fibre/matrix interface. The light and dark grey phases represent ZrB_2 and SiC respectively. The carbon fibres are black.

For ZS system it is hypothesized that densification was mainly driven by solid state mechanisms due to C phases spread in the matrix that cleaned the surface of ZrB_2 particles from residual oxides. The efficacy of carbon is well evident at the fibre/matrix interface where we can recognize a localized area of about 1 micron thick fully densified, while far from the fibre the matrix is more porous. Moreover, we cannot exclude the local formation of small amounts of liquid phase originating from residual silica and boria present on the starting powder particles.

Sample ZSY:

This composite was characterized by a significantly lower porosity (<1%) than ZS (8.2%) owing to the formation of a lower melting liquid phase that aided the sintering of ZrB_2. This was accompanied by an increase of ZrB_2 grain size of 50% (from 2.4 to 3.6 μm) [17].

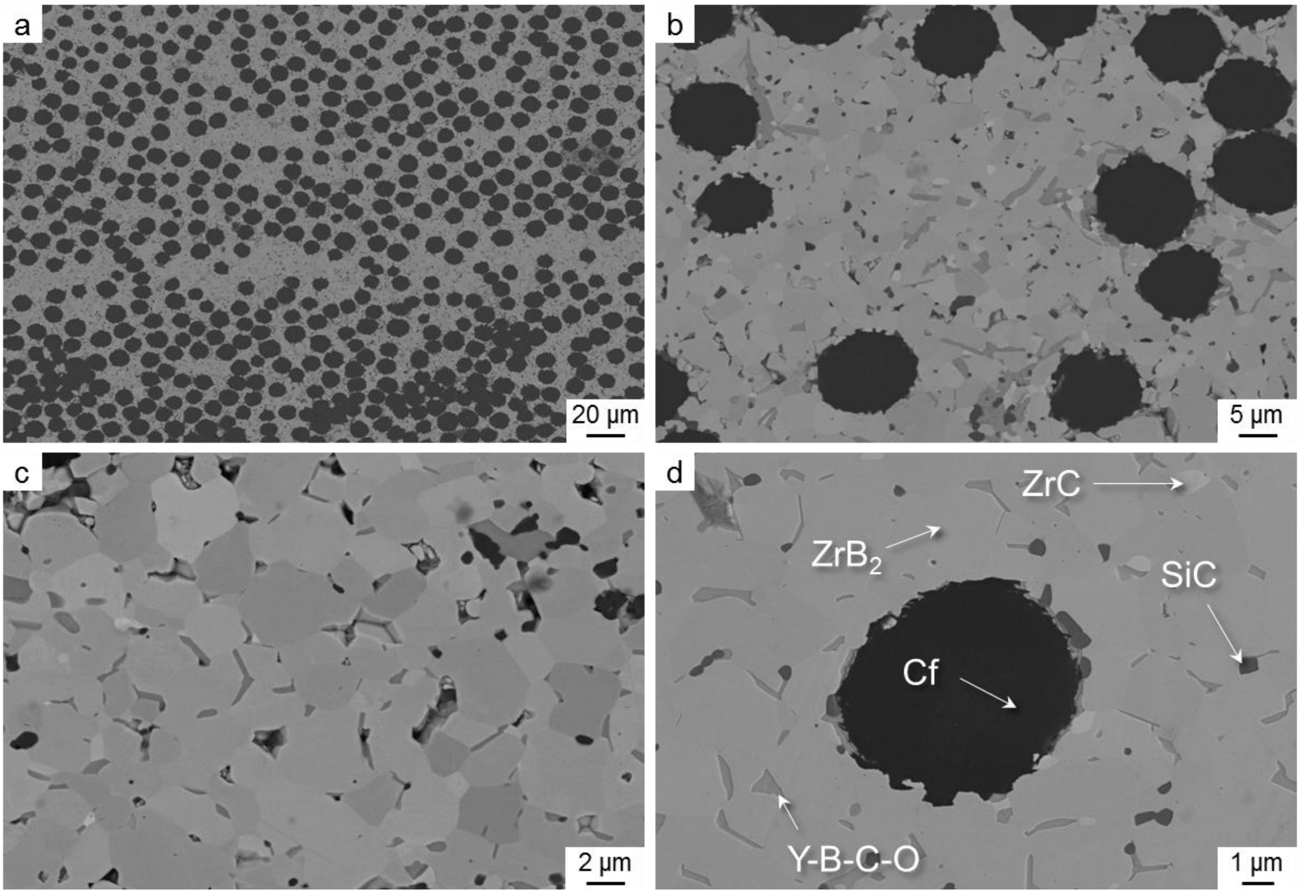

Figure 2. SEM micrographs of ZSY: a) Fibre distribution, b) microstructure and phases distribution, c) detail of the UHTC matrix, d) Fibre/matrix interface. The four shades of grey, going from the lightest to the darkest, represent ZrC, Y-B-C-O phases, ZrB_2 and SiC respectively. The carbon fibres are black.

For the ZSY system the densification behaviour was rather different. The matrix was fully dense, the ZrB_2 grain coarsening suggests dissolution and re-precipitation mechanisms and additional phase formation is observed at the matrix/fibre interface (fig. 2b,d). All these mechanisms indicate a liquid phase sintering mechanism. According to the SiO_2-Y_2O_3 phase diagram [23], a eutectic liquid phase may form at ~1650°C, between yttria and silica impurities. This liquid was also likely enriched with B_2O_3 present on the surface of ZrB_2 particles. The miscellaneous Y-Si-B-O liquid phase spread in the matrix and at the fibre/matrix interface, helping rearrangement and dissolution of ZrB_2, diffusion and re-precipitation. The improvement of densification for ZrB_2-SiC systems doped with Y_2O_3 was reported by other authors and was attributed to the ability of Y_2O_3 to form liquid phases with the oxide impurities present on the boride and carbide particles, resulting in the strengthening of grain boundaries [17]. However, in the present study, the presence of carbon fibres complicated the picture. Indeed, during re-precipitation from the liquid phase, different phases could form depending on the local chemistry, e.g. the local availability of C or O could cause the formation of prevalently oxides, prevalently carbides or mixed oxy-carbides, as observed by EDS analyses. On closer inspection (fig 3), these phases were mainly comprised of Y, B, C and O with varying ratios, while Si signal was hardly found. These phases were characterized by a lamellar structure with features similar to rare earth borocarbides such as YB_2C_2 (T_m > 2200 K) [24][25][26][27] and were likely originated from the reduction of Y_2O_3 and the B_2O_3 present on the surface of ZrB_2 particles with the carbon of the fibres or fibre debris [26][25]. Hypothesized reactions that lead to the formation of said phases are reported below:

$$Y_2O_3 + 2\ SiO_2 \rightarrow Y_2Si_2O_7 \qquad (1)$$

$$Y_2O_3 + B_2O_3 \rightarrow 2\ YBO_3 \qquad (2)$$

$$Y_2O_3 + 2\ B_2O_3 + 13\ C \rightarrow 2\ YB_2C_2 + 9\ CO \qquad (3)$$

$$C + Y_2O_3 \rightarrow YC_2 + CO \qquad (4)$$

XRD analysis was carried out on the as produced composite (not shown); the main phases were indexed to ZrB_2 and SiC 6H, but minor unidentified phases were observed at high 2θ. However further analysis is needed for a more accurate assessment of these phases structure and characteristics.

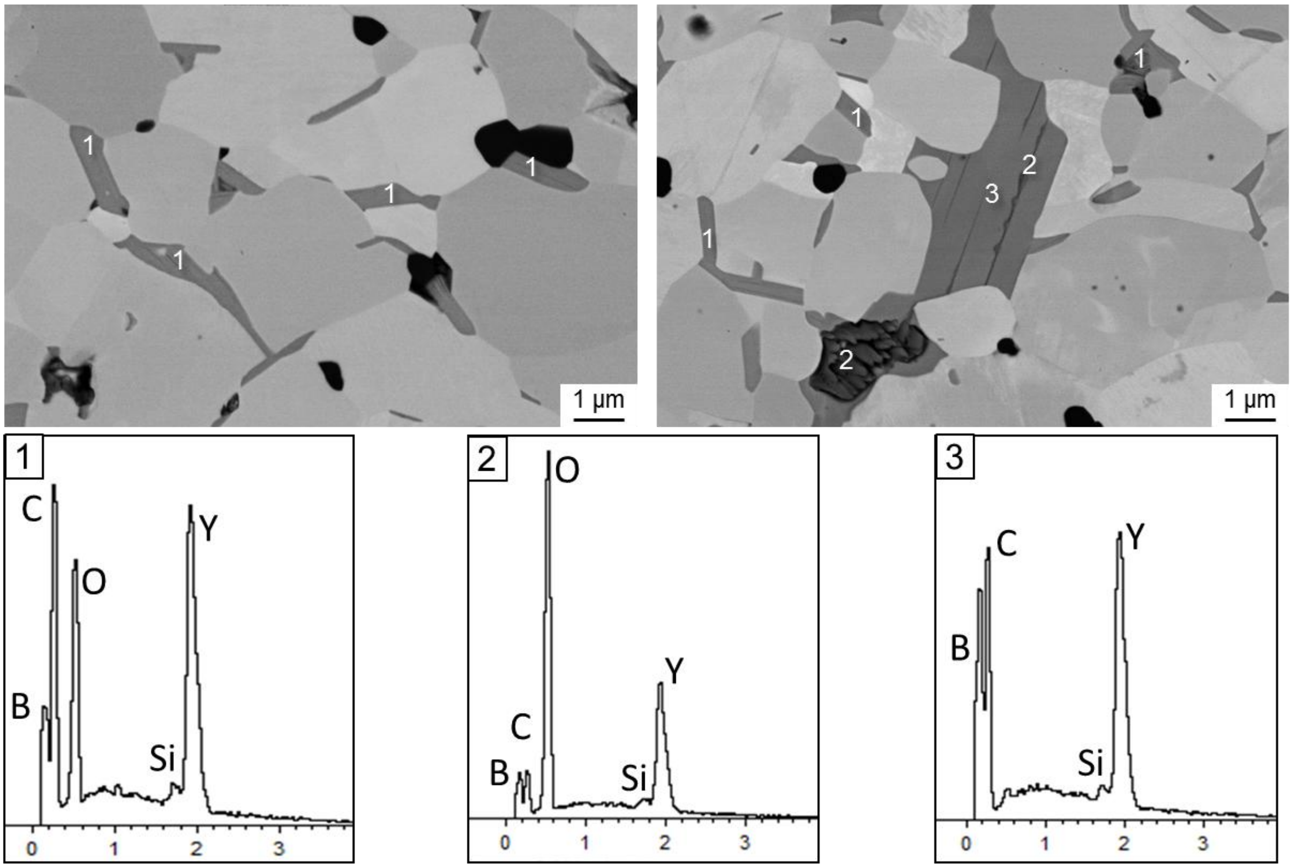

Figure 3. High magnification SEM micrographs of the UHTC matrix of ZSY showing the Y-B-C-O phases with varying stoichiometry and the respective EDS spectra collected at 5 keV. The light grey and black phases are ZrB_2 and SiC, the white particles are ZrC and the dark grey phases are Y-B-C-O phases. Si signal was occasionally detected in these phases.

3.2 Mechanical properties

The values of strength and fracture toughness at room temperature were 283 MPa and 8.00 $MPam^{0.5}$ for ZS and 436 MPa and 11.5 $MPam^{0.5}$ for ZSY respectively (Table 2). The bending strength of fibre-reinforced UHTC composites was found to be lower than the corresponding bulk ceramics [28]. This could be attributed to micro-cracks generated during cooling from the densification temperature due to the CTE mismatch between the fibres and the matrix [29] or the early inter-laminar shear failure of the specimens under bending. The strength values obtained in this work were used for comparison purposes.

Table 2: 4-point flexural strength values from RT to 1500°C and fracture toughness evaluated with the chevron notch beam test of ZS and ZSY.

Sample	σ (MPa)	$\sigma_{1200°C}$ (MPa)	$\sigma_{1500°C}$ (MPa)	K_{Ic} ($MPam^{0.5}$)
ZS	283 ± 23	-	-	8.0 ± 0.9
ZSY	436 ±20	607 ± 23	709 ± 88	11.5 ± 0.7

The strength and fracture toughness of ZS were comparable with those of UHTCMCs studied in previous works [30][31] that were in the range of 280 – 350 MPa and 8 – 11 $MPam^{0.5}$, respectively, whereas the properties of ZSY were significantly higher (436 MPa and 11.5 $MPam^{0.5}$ respectively). The higher performance of ZSY can be attributed to the stronger grain boundaries and denser matrix, as well as the slightly higher fibre content. The slope of the load-displacement curves relative to the flexural strength of ZS experiences a small decrease which is typically attributed to a weak fibre/matrix interface and the premature failure of the matrix (fig. 4). Initially stresses were mostly concentrated in the ceramic matrix. With the increase of the applied load, cracks started to open in the ceramic matrix and the load was transferred to the fibres. For ZSY this effect is negligible, indicating a stronger fibre/matrix interaction.

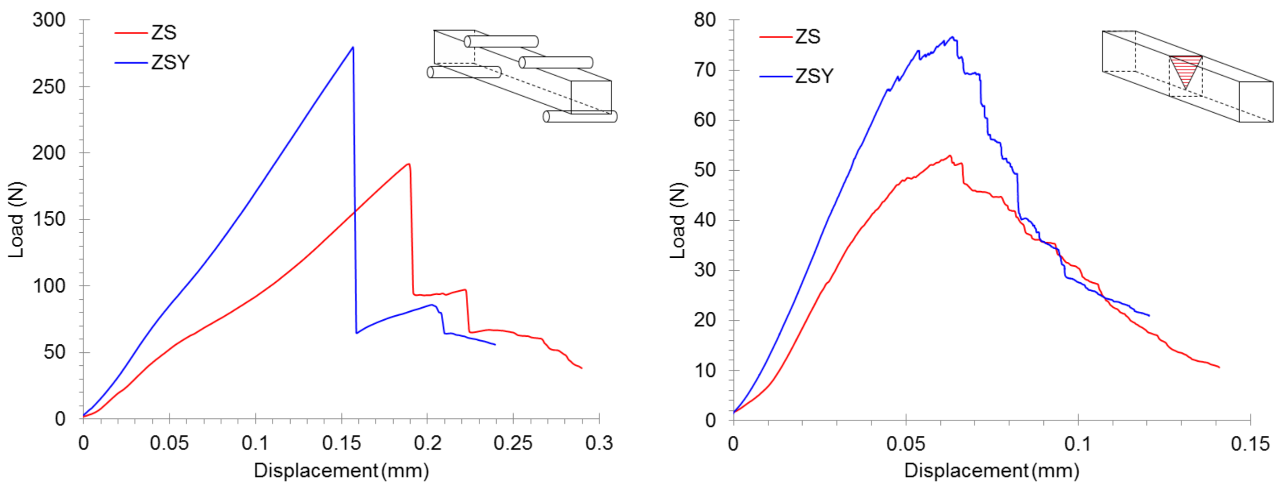

Figure 4. Load displacement curves for the 4-point flexural strength and fracture toughness of ZS and ZSY measured at room temperature.

ZSY strength was further investigated at high temperature. Strength increased from 436 to 607 MPa at 1200°C; this was attributed to the relaxation of residual stresses accumulated during hot pressing [29][30]. At

1500°C, strength increased further to 709 MPa, which is the highest value ever reported for this class of materials. A slight plastic deformation was observed in proximity of the maximum applied load. Due to inaccuracy of the apparatus in measuring the true strain of the load-displacement, the true strength of the material was considered reliable up to the proportional limit in the curve. This was calculated using the maximum load in the elastic region which was determined from the best fit of the linear portion of the load/displacement curves (fig. 5), which had R^2 values of 0.998. The calculated strength at the proportional limit was 516 MPa, which was slightly lower than the strength registered at 1200°C but still higher than the RT value, while retaining an ultimate strength of 709 MPa. Compared to previously studied composites based on a TaC and HfC matrix, ZrB_2 based composites yielded at lower temperatures [11][12]. This could be attributed to the presence of residual low melting phases deriving from the sintering process [17]. In any case, the strength reached is well above

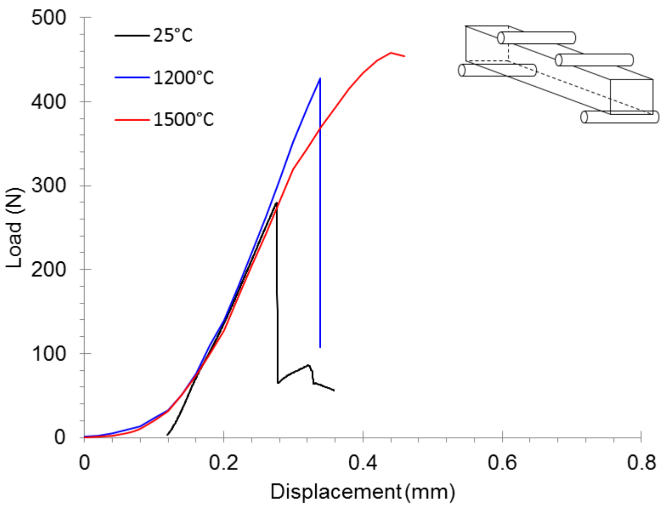

Figure 5. Load displacement curves for the 4-point flexural strength of ZSY measured at RT, 1200°C and 1500°C.

Looking at the fracture surfaces of ZS and ZSY, limited fibre pull-out was observed in both specimens (fig. 6 a,d), amounting to only 5-20 µm. ZSY displays a more compact and dense ceramic matrix (fig. 6b,e), but in both composites the first layers of the pitch fibre were anchored to the ceramic matrix (fig. 6c,f). In the case of ZSY this effect was more dominant and in accordance with the load-displacement curves discussed before.

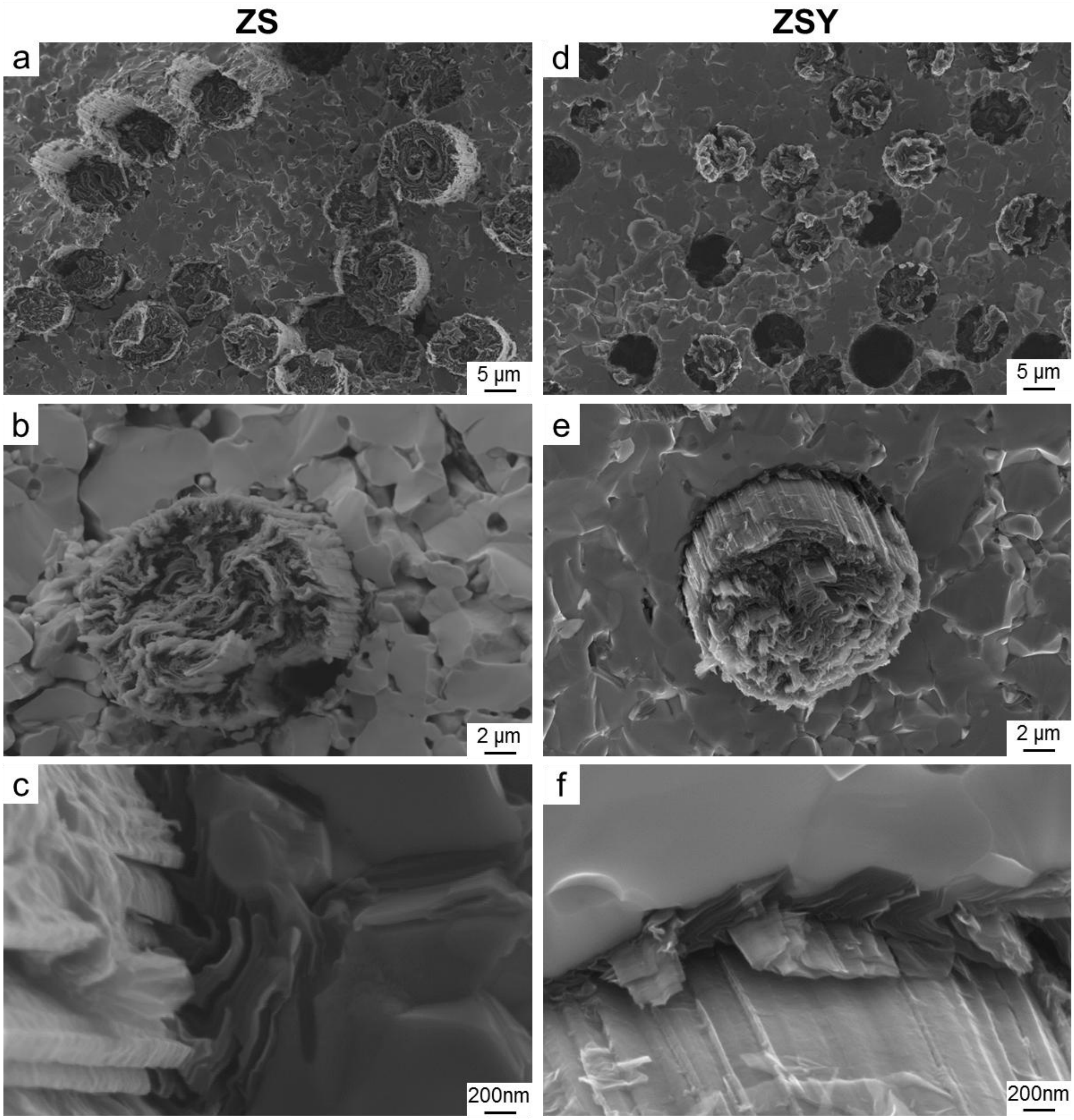

Figure 6. Fracture surfaces of ZS and ZSY after bending tests at RT: a,d) fracture surfaces, b,e) High magnification of the fibre, c, f) Fibre/matrix interface

3.3 Oxidation Tests

X-Ray diffraction analysis was carried out after testing at 1500 and 1650°C in order to identify the species that formed on the surface during oxidation (Fig. 7). In all XRD patterns the highest peak was attributed to hydrated boron oxide, $B(OH)_3$ (PDF#30-0199), which formed on the surface of the specimens after testing due to contact with air humidity. The main phase after oxidation was monoclinic ZrO_2 for both specimens (PDF#86-1449). No tetragonal or cubic ZrO_2 were detected. A small peak relative to silicon species (PDF#83-2187) was detected at 1500°C for both samples, but it is not visible at 1650°C, likely due to the partial evaporation and amorphous nature of the silica layer. For ZSY, additional peaks were indexed to YBO_3 formation (PDF#88-0356).

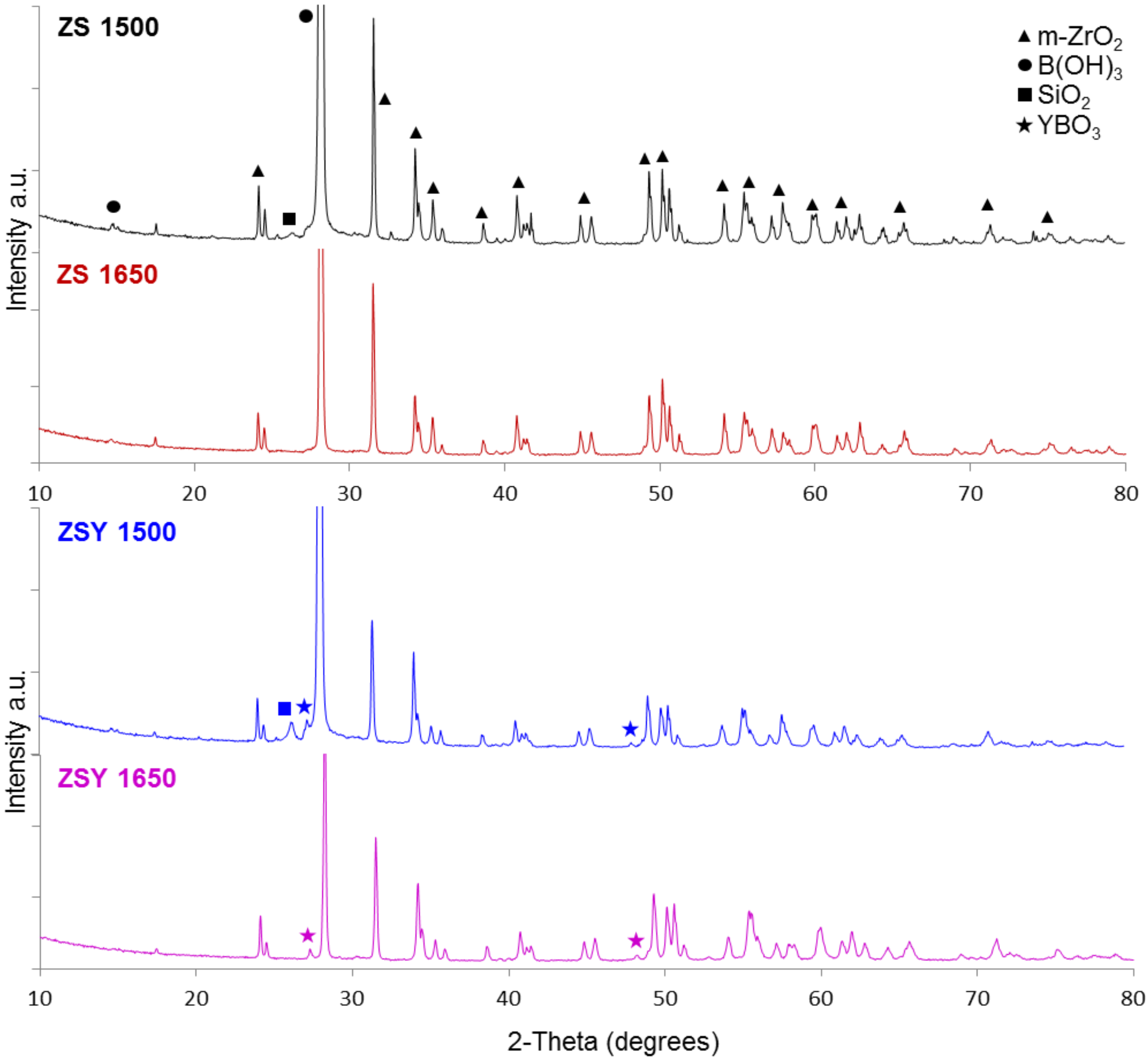

Figure 7. X-Ray diffraction patterns of samples ZS and ZSY after oxidation at 1500 and 1650°C in air. The main peaks are relative to monoclinic ZrO_2 (PDF#86-1449), SiO_2 (PDF#83-2187). Small peaks relative to YBO_3 formation were observed for sample ZSY (PDF#88-0356).

Following XRD characterization, SEM analysis was carried out on the surface and cross section of the oxidized samples. After testing at 1500°C, the surface of ZS is characterized by small ZrO_2 grains embedded in a glassy silica layer (fig. 8a), while that of ZSY is characterized by large ZrO_2 grains surrounded by a glassy phase containing Y, B, O (fig. 8d) and small amounts of Si, which was attributed to the formation of YBO_3 originating from the oxidation of the Y-B-C-O phases found in the bulk composite. The cross-section of ZS is characterized mainly by two regions as reported previously by the same authors [13][14]: an outer silica layer and an intermediate scale of columnar ZrO_2 + SiO_2 (fig. 8b). For ZSY only one scale was observed, mainly consisting of ZrO_2 grains held together by a glassy phase of SiO_2 and YBO_3 (fig. 8e). This glassy phase was more abundant near the surface. In the case of ZS, the outer fibres were removed due to the oxidation of the carbon to CO (fig. 8c), while for ZSY the outer fibres were still mostly intact due to the rapid action of the borate that quickly protected them from oxidation (fig. 8f). The thickness of the oxidized layer of ZS (18 μm) was comparable to that of ZSY (24 μm) and was thinner than that reported in previous works [14].

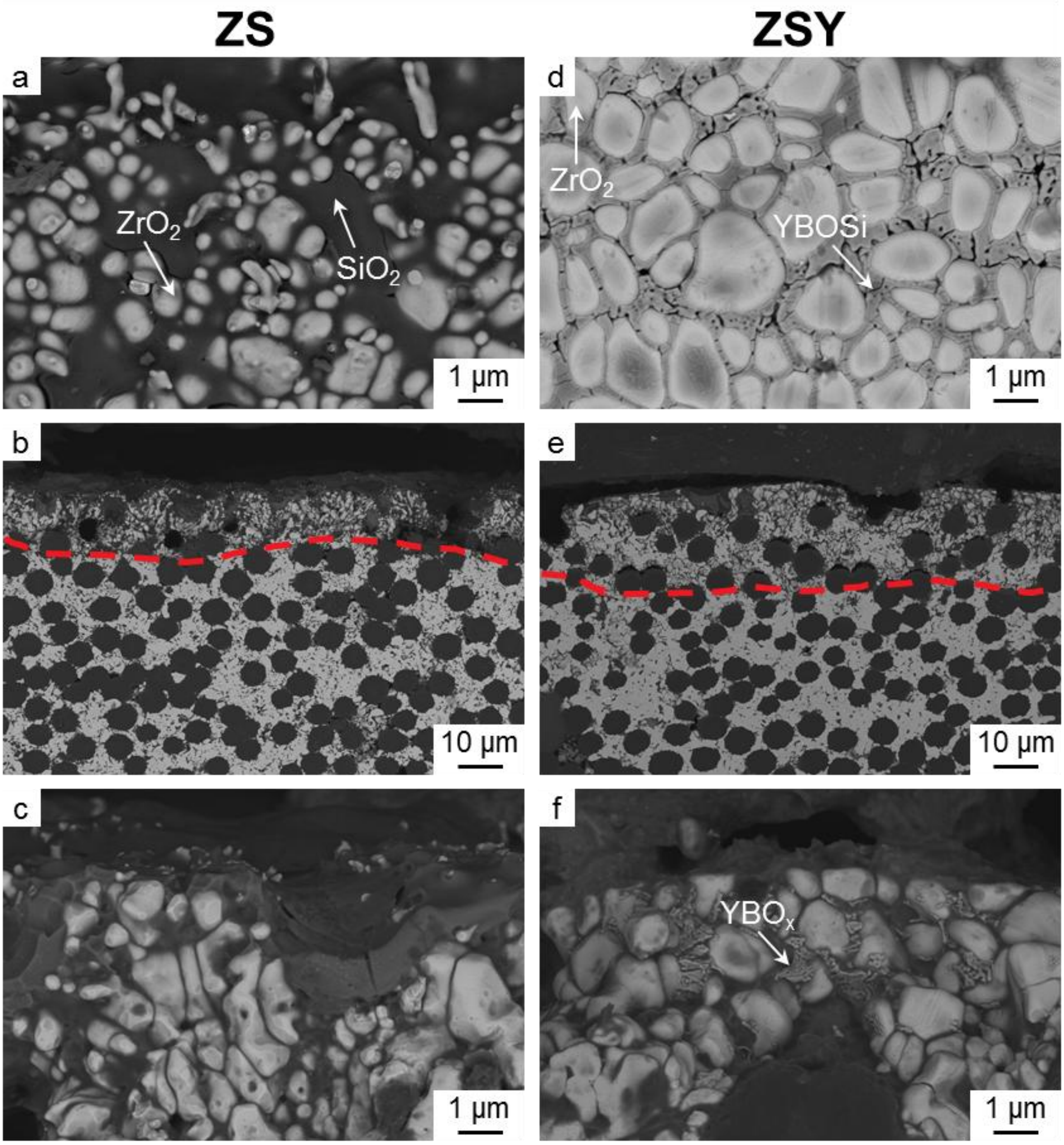

Figure 8. Microstructure of ZS and ZSY after oxidation at 1500°C in air: a,d) surface morphology, b,e) cross-section of the oxidized layer, c,f) detail of the oxidized layer.

After oxidation at 1650°C, the specimens were visibly more damaged (fig. 9b,e). The surface of ZS was similar to that observed at 1500°C, with zirconia grains growing from the silica melt (fig. 9a), but the oxidized layer was thicker (43 µm, fig. 9c). The surface of ZSY was very different: the silica layer, which was barely visible at 1500°C, was now more abundant on the surface (fig. 9d), while the intermediate layer consisted mainly of a porous ZrO_2 – SiO_2 – YBO_3 scale (fig. 9e). Some YBOSi phase was still found at ZrO_2 grain boundaries (fig. 9a,c). The oxidized layer of ZSY increased to 53 μm and was prone to detachment due to an inner porous layer originating from the oxidation of the outer fibres. The morphology of the ZrO_2 is also different: for ZS columnar ZrO_2 was observed (fig. 9c), while for ZSY the ZrO_2 grains were larger and rounded (fig. 9f).

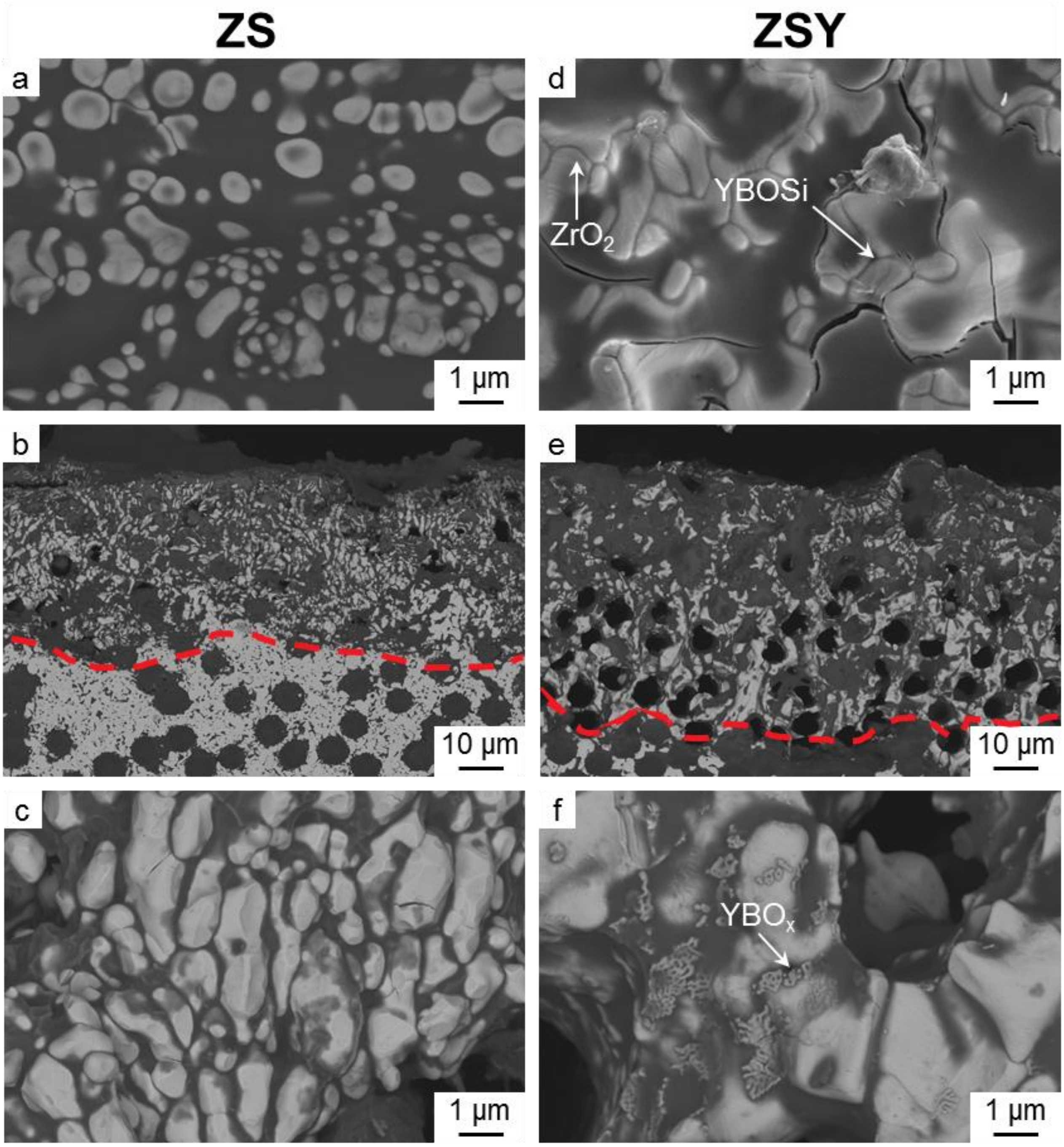

Figure 9. Microstructure of ZS and ZSY after oxidation at 1650°C in air: a,d) surface morphology, b,e) cross-section of the oxidized layer, c,f) detail of the oxidized layer.

Previous studies on fibre reinforced ZrB_2/SiC with varying SiC contents showed how the oxidation resistance increased with SiC content [14], showing optimal results for SiC > 10%. Even though Y_2O_3 played a significant role during the densification process and improved the mechanical properties, it also deprived the composite from SiC as ascertained from image analysis on the sintered specimen. The Y-B-O phase was well spread around the ZrO_2 grains but there was not enough SiO_2 production to fully cover and protect the composite from further oxidation, resulting in a slightly lower oxidation resistance than the un-doped specimen. Other works on the kinetics of oxidation of ZrB_2/SiC composites showed three main reactions that take place during oxidation [13]:

$$C + \frac{1}{2} O_2 \rightarrow CO_{(g)} \quad (1)$$

$$C + O_2 \rightarrow CO_{2(g)} \quad (2)$$

$$ZrB_2 + 5O_2 \rightarrow ZrO_{2(s)} + B_2O_{3(l,g)} \quad (3)$$

$$SiC + 3/2O_2 \rightarrow SiO_{2(l)} + CO_{(g)} \quad (4)$$

Carbon started oxidizing at temperatures as low as 500°C, while ZrB_2 oxidation started at around 800°C. The oxidation of SiC to SiO_2 is triggered at higher temperatures (T > 1000°C) and usually leads to the formation of a protective layer on the surface of the composite. For ZSY additional reactions occurred that led to the formation of YBO_x glasses. These are thought to originate from the oxidation of the Y-B-C or Y-B-C-O phases identified in the bulk.

Conclusions

The influence of Y_2O_3 on the microstructure, thermo-mechanical properties and oxidation resistance of carbon fibre reinforced ZrB_2/SiC composites was investigated. Y_2O_3 was initially added with the goal of improving the oxidation resistance by enhancing the sintering process and promoting the formation of a more compact ZrO_2 layer during oxidation. As far as the sintering process is concerned, Y_2O_3 led to the formation of liquid phases with impurity oxides that aided the sintering of the UHTC phase. However, the presence of carbon in the system led to additional reactions that resulted in the consumption of Y_2O_3 and formation of yttrium boro-carbides, which was accompanied by the partial removal of SiC. The formation of these novel phases at the fibre/matrix interface led to very strong interfaces and resulted in higher stiffness and a significant increase of the mechanical properties that were 50% higher than the undoped composite (strength up to 700 MPa at 1500°C and fracture toughness of 12 $MPam^{0.5}$).

After oxidation at 1500°C in air, ZS was characterized by an outer silica layer and an intermediate ZrO_2/SiO_2 scale, while ZSY was characterized by large ZrO_2 grains surrounded by yttrium borate on the surface, and an inner layer of $ZrO_2/SiO_2/YBO_3$. The oxide layer thickness was comparable and no significant improvement of the oxidation resistance was observed.

After oxidation at 1650°C, the doped sample displayed inferior oxidation resistance; the outer layer visibly more damaged and the intermediate layer is very porous. This was attributed to the partial evaporation of low melting phases coupled with an overall lower SiC content that resulted in insufficient formation of the protective silica layer.

Acknowledgements

This work has received funding from the European Union's Horizon 2020 "Research and innovation programme" under grant agreement N°685594 (C^3HARME).

The authors are grateful to Cesare Melandri for mechanical testing, Daniele Dalle Fabbriche for hot pressing and Mauro Mazzocchi for XRD analysis.

- The raw/processed data required to reproduce these findings cannot be shared at this time due to technical or time limitations.

References

[1] Levine SR, Opila EJ, Halbig MC, Kiser JD, Singh M, Salem JA. Evaluation of ultra-high temperature ceramics for aeropropulsion use. J Eur Ceram Soc 2002;22:2757–67. doi:10.1016/S0955-2219(02)00140-1.

[2] Opeka MM, Talmy IG, Wuchina EJ, Zaykoski J a., Causey SJ. Mechanical, Thermal, and Oxidation Properties of Refractory Hafnium and zirconium Compounds. J Eur Ceram Soc 1999;19:2405–14. doi:10.1016/S0955-2219(99)00129-6.

[3] Sha JJ, Li J, Wang SH, Zhang ZF, Zu YF, Flauder S, et al. Improved microstructure and fracture properties of short carbon fiber-toughened ZrB2-based UHTC composites via colloidal process. Int J Refract Met Hard Mater 2016;60:68–74. doi:10.1016/j.ijrmhm.2016.07.010.

[4] Walker LS, Corral EL. Self-Generating High-Temperature Oxidation-Resistant Glass-Ceramic Coatings for C–C Composites Using UHTC s. J Am Ceram Soc 2014;97:3004–11. doi:10.1111/jace.13017.

[5] A. Paul, D.D. Jayaseelan, S. Venugopal, E. Zapata-Solvas, J. Binner, B. Vaidhyanathan, A. Heaton, P. Brown WEL, UHTC. UHTC-composites for hypersonic applications. Am Ceram Soc Bull 2012;91:22.

[6] Tang S, Deng J, Wang S, Liu W, Yang K. Ablation behaviors of ultra-high temperature ceramic composites. Mater Sci Eng A 2007;465:1–7. doi:10.1016/j.msea.2007.02.040.

[7] Tang S, Deng J, Wang S, Liu W. Comparison of thermal and ablation behaviors of C/SiC composites and C/ZrB2-SiC composites. Corros Sci 2009;51:54–61. doi:10.1016/j.corsci.2008.09.037.

[8] Sciti D, Natali Murri A, Medri V, Zoli L. Continuous C fibre composites with a porous ZrB2 Matrix. Mater Des 2015;85:127–34. doi:10.1016/j.matdes.2015.06.136.

[9] Sciti D, Pienti L, Natali Murri A, Landi E, Medri V, Zoli L. From random chopped to oriented continuous SiC fibers-ZrB2 composites. Mater Des 2014;63:464–70. doi:10.1016/j.matdes.2014.06.037.

[10] Zoli L, Sciti D. Efficacy of a ZrB2–SiC matrix in protecting C fibres from oxidation in novel UHTCMC materials. Mater Des 2017;113:207–13. doi:10.1016/j.matdes.2016.09.104.

[11] Vinci A, Zoli L, Sciti D, Watts J, Hilmas GE, Fahrenholtz WG. Mechanical behaviour of carbon fibre

reinforced TaC/SiC and ZrC/SiC composites up to 2100°C. J Eur Ceram Soc 2018;39:780–7. doi:10.1016/J.JEURCERAMSOC.2018.11.017.

[12] Vinci A, Zoli L, Sciti D, Watts J, Hilmas GE, Fahrenholtz WG. Influence of fibre content on the strength of carbon fibre reinforced HfC/SiC composites up to 2100°C. J Eur Ceram Soc 2019;39:3594–603. doi:10.1016/j.jeurceramsoc.2019.04.049.

[13] Vinci A, Zoli L, Landi E, Sciti D. Oxidation behaviour of a continuous carbon fibre reinforced ZrB2–SiC composite. Corros Sci 2017;123:129–38. doi:10.1016/j.corsci.2017.04.012.

[14] Vinci A, Zoli L, Sciti D. Influence of SiC content on the oxidation of carbon fibre reinforced ZrB2/SiC composites at 1500 and 1650 °C in air. J Eur Ceram Soc 2018;38:3767–76. doi:10.1016/j.jeurceramsoc.2018.04.064.

[15] Mungiguerra S, Martino GD Di, Cecere A, Savino R, Silvestroni L, Vinci A, et al. Arc-jet wind tunnel characterization of ultra-high-temperature ceramic matrix composites. Corros Sci 2019;149:18–28. doi:https://doi.org/10.1016/j.corsci.2018.12.039.

[16] Zoli L, Vinci A, Galizia P, Gutièrrez-Gonzalez CF, Rivera S, Sciti D. Is spark plasma sintering suitable for the densification of continuous carbon fibre - UHTCMCs? J Eur Ceram Soc 2019. doi:https://doi.org/10.1016/j.jeurceramsoc.2019.12.004.

[17] Zhang X, Li X, Han J, Han W, Hong C. Effects of Y2O3 on microstructure and mechanical properties of ZrB2-SiC ceramics. J Alloys Compd 2008;465:506–11. doi:10.1016/j.jallcom.2007.10.137.

[18] Guo W-M, Vleugels J, Zhang G-J, Wang P-L, der Biest O. Effects of Re2O3 (Re = La, Nd, Y and Yb) addition in hot-pressed ZrB2–SiC ceramics. J Eur Ceram Soc 2009;29:3063–3068. doi:10.1016/j.jeurceramsoc.2009.04.021.

[19] Li W, Zhang X, Hong C, Han J, Han W. Hot-pressed ZrB2–SiC–YSZ composites with various yttria content: Microstructure and mechanical properties. Mater Sci Eng A 2008;494:147–52. doi:https://doi.org/10.1016/j.msea.2008.04.010.

[20] Vinci A, Zoli L, Sciti D, Melandri C, Guicciardi S. Understanding the mechanical properties of novel UHTCMCs through random forest and regression tree analysis. Mater Des 2018;145. doi:10.1016/j.matdes.2018.02.061.

[21] Munz DG, Shannon JL, Bubsey RT. Fracture toughness calculation from maximum load in four point

bend tests of chevron notch specimens. Int J Fract 1980;16. doi:10.1007/BF00013393.

[22] Lee Y-J. Formation of silicon carbide on carbon fibers by carbothermal reduction of silica. Diam Relat Mater 2004;13:383–8. doi:10.1016/j.diamond.2003.11.062.

[23] Hnatko M, Šajgalík P, Lenčéš Z, Salamon D, Monteverde F. Carbon reduction reaction in the Y2O3–SiO2 glass system at high temperature. J Eur Ceram Soc 2001;21:2797–801. doi:10.1016/S0955-2219(01)00231-X.

[24] Tanaka T, Sato A, Watanabe K, Nagao M. Related content Novel ternary Y-B-C compound : Y 10 + x B 7 C 10-x (x ≈ 2009:0–8. doi:10.1088/1742-6596/176/1/012006.

[25] Zhao G, Chen J, Li Y, Li M. YB2C2: A machinable layered ternary ceramic with excellent damage tolerance. Scr Mater 2016;124:86–9. doi:10.1016/j.scriptamat.2016.06.041.

[26] Zhou Y, Xiang H, Wang X, Sun W, Dai FZ, Feng Z. Electronic structure and mechanical properties of layered compound YB2C2: A promising precursor for making two dimensional (2D) B2C2 nets. J Mater Sci Technol 2017;33:1044–54. doi:10.1016/j.jmst.2016.09.028.

[27] Yang Y, Hong T. Mechanical and thermodynamic properties of YB2C2 under pressure. Phys B Condens Matter 2017;525:154–8. doi:https://doi.org/10.1016/j.physb.2017.09.026.

[28] Monteverde F, Guicciardi S, Melandri C, Fabbriche DD. Densification, Microstructure Evolution and Mechanical Properties of Ultrafine SiC Particle-Dispersed ZrB2 Matrix Composites. In: Orlovskaya N, Lugovy M, editors. Boron Rich Solids, Dordrecht: Springer Netherlands; 2011, p. 261–72.

[29] Galizia P, Zoli L, Sciti D. Impact of residual stress on thermal damage accumulation, and Young's modulus of fiber-reinforced ultra-high temperature ceramics. Mater Des 2018;160:803–9. doi:https://doi.org/10.1016/j.matdes.2018.10.019.

[30] Zoli L, Vinci A, Galizia P, Melandri C, Sciti Di. On the thermal shock resistance and mechanical properties of novel unidirectional UHTCMCs for extreme environments. Sci Rep 2018;8:1–9. doi:10.1038/s41598-018-27328-x.

[31] Galizia P, Failla S, Zoli L, Sciti D. Tough salami-inspired Cf/ZrB2 UHTCMCs produced by electrophoretic deposition. J Eur Ceram Soc 2018;38:403–9. doi:10.1016/J.JEURCERAMSOC.2017.09.047.